Extended Optical Model Analyses of Elastic Scattering, Direct Reaction, and Fusion Cross Sections for the ^{9}Be+^{208}Pb System at Near-Coulomb-Barrier Energies

W. Y. So

Laboratory of Cyclotron Application,

Korea Institute of Radiological and Medical Sciences, Seoul 139-706, Korea

S. W. Hong, and B. T. Kim

Department of Physics and Institute of Basic Science,

Sungkyunkwan University, Suwon 440-746, Korea

T. Udagawa

Department of Physics, University of Texas, Austin, Texas 78712

Abstract

Based on the extended optical model approach in which the polarization potential is decomposed into direct reaction (DR) and fusion parts, simultaneous χ^2 analyses are performed for elastic scattering, DR, and fusion cross section data for the ^{9}Be+^{208}Pb system at near-Coulomb-barrier energies. Similar χ^2 analyses are also performed by only taking into account the elastic scattering and fusion data as was previously done by the present authors, and the results are compared with those of the full analysis including the DR cross section data as well. We find that the analyses using only elastic scattering

and fusion data can produce very consistent and reliable predictions of cross sections particularly when the DR cross section data are not complete. Discussions are also given on the results obtained from similar analyses made earlier for the ^{9}Be+^{209}Bi system.

PACS numbers : 24.10.-i, 25.70.Jj

I. INTRODUCTION

In our recent study [1], we have carried out simultaneous χ^2 analyses of elastic scattering and fusion cross section data for the ^{6}Li+^{208}Pb [2, 3, 4] and ^{9}Be+^{209}Bi [5, 6] systems at near-Coulomb-barrier energies in the framework of an extended optical model [7, 8, 9] by introducing two types of complex polarization potentials: the direct reaction (DR) and fusion potentials. In such analyses, it is indispensable and essential to include the experimental data for the total DR cross section σ_D^{exp} and the fusion cross section σ_F^{exp}, in addition to the elastic scattering cross section $d\sigma_E^{exp}/d\Omega$ for the separate determination of the DR and fusion potentials. However, when the previous study was made [1], reliable data of σ_D^{exp} for ^{6}Li+^{208}Pb and ^{9}Be+^{209}Bi were not available, and thus the analyses were proceeded in two steps. In the first step, we carried out χ^2 analyses of only the elastic scattering data by assuming just one simple Woods-Saxon type complex potential. Using the potential parameters thus fixed, we could then generate the total reaction cross section σ_R, which we called the semi-experimental total reaction cross section $\sigma_R^{semi-exp}$. As has been shown in a number of publications, such $\sigma_R^{semi-exp}$ predicted from the optical potential that fits the elastic scattering data usually reproduces σ_R^{exp} very well. This is the case for reactions induced by the proton [10, 11], the deuteron [12], the α-particle [13], and also heavy-ions [14]. We then used $\sigma_R^{semi-exp}$ to further extract semi-experimental total DR cross sections $\sigma_D^{semi-exp}$ by using the relation $\sigma_D^{semi-exp} = \sigma_R^{semi-exp} - \sigma_F^{exp}$. In the second step, use was made of thus extracted $\sigma_D^{semi-exp}$ in place of the experimental DR cross section σ_D^{exp} to carry out simultaneous analyses of $d\sigma_E^{exp}/d\Omega$, $\sigma_D^{semi-exp}$, and σ_F^{exp} for determining the full extended optical model potential composed of two polarization potentials.

The DR and fusion potentials thus determined revealed interesting characteristic fea-

tures of these potentials. First of all, both potentials satisfy separately the dispersion relation [15]. Secondly, the fusion potential is found to exhibit a threshold anomaly [15, 16], as was observed for tightly bound projectiles [17, 18, 19], but the DR potential does not show a pronounced threshold anomaly. Thirdly at the strong absorption radius, the magnitudes of the fusion potential were found to be much smaller than those of the DR potential. As a consequence, the resulting total polarization potential dominated by the DR potential becomes rather smooth as a function of the incident energy. This has solved a long standing puzzle why the threshold anomaly has not been seen in the polarization potentials determined for the systems involving a loosely bound projectile such as ^{6}Li and ^{9}Be [2, 5].

The extracted DR potentials have provided us with a unique opportunity to study the effects of breakup (DR) on fusion by comparing σ_F calculated from either including or neglecting the real and the imaginary part of the DR potential. Such studies were made in Ref. [1], which showed that in the sub-barrier region, breakup is not the main reason for the subbarrier enhancement of σ_F^{exp} and that the mechanism that governs the enhancement is neutron flow as originally suggested by Stelson *et al.* [20]. In our approach, this effect is phenomenologically implemented in the imaginary part of the DR potential. On the other hand, in the above barrier region, the breakup suppresses σ_F^{exp} and the observed suppression factors for ^{6}Li and ^{9}Be were fairly well accounted for in terms of the breakup [1].

After completing our work of Ref. [1] for ^{9}Be + ^{209}Bi system, elastic scattering data for ^{9}Be + ^{208}Pb, a system similar to ^{9}Be + ^{209}Bi, have become available [21]. Thus, for ^{9}Be + ^{208}Pb system we now have data available for the elastic scattering [21] and fusion [22] cross sections as well as the sum of cross sections of breakup, transfer, and incomplete

fusion [23]. For a loosely bound projectile like ^{9}Be, we may assume the summed cross section thus observed as the total DR cross sections. This has provided us with an opportunity to carry out χ^2 analyses taking into account all three sets of experimental data, i.e., the elastic scattering, DR, and fusion data. We can then compare these χ^2 analysis results with those obtained by considering only two sets of data, i.e., the elastic scattering and fusion data without the experimental DR data. We shall henceforth call the case where all the three data sets are included in the χ^2 analyses the EDF (elastic, DR, and fusion) approach, and the case where only two data sets are considered the EF (elastic scattering and fusion) approach. Note that in the EF approach we do, however, include $\sigma_D^{semi-exp}$, which is essential to fix the DR potential parameters. The aim of the present study is to make a comparison between these two approaches and study the validity of the EF method used in our previous work. By extending our EF method proposed in the previous work on ^{9}Be + ^{209}Bi to ^{9}Be + ^{208}Pb system, where we have DR data as well as elastic and fusion data, we shall show that the EF approach gives us very reliable predictions of cross sections.

In Sec. II, we first generate $\sigma_D^{semi-exp}$ for the EF approach case by following the method described in Ref. [1]. Two types of χ^2 analyses (EDF and EF) are then carried out in Sec. III and the results are compared and discussed in Sec. IV. Sec. V concludes the paper.

II. EXTRACTING SEMI-EXPERIMENTAL DR CROSS SECTION

Our method of generating $\sigma_D^{semi-exp}$ resorts to the empirical fact [24] that the total reaction cross section calculated from the optical model fit to the available elastic scattering cross section data, $d\sigma_E^{exp}/d\Omega$, usually agrees well with the experimental σ_R, in

spite of the well known ambiguities in the optical potential. Let us call the total reaction cross section thus generated the semi-experimental reaction cross section $\sigma_R^{semi-exp}$. Then, $\sigma_D^{semi-exp}$ is generated by

$$\sigma_D^{semi-exp} = \sigma_R^{semi-exp} - \sigma_F^{exp}. \tag{1}$$

This approach seems to work even for loosely bound projectiles, as demonstrated recently by Kolata *et al.* [14] for the ^{6}He+^{209}Bi system.

Following Ref. [1], we first carry out rather simple optical model χ^2 analyses of elastic scattering data solely for the purpose of deducing $\sigma_R^{semi-exp}$. For these preliminary analyses, we assume the optical potential to be a simple sum of two volume-type potentials $V_0(r)$ and $U_1(r, E)$, where $V_0(r)$ is the real, energy independent bare potential and $U_1(r, E)$ is a complex potential with common geometrical parameters for both real and imaginary parts. The elastic scattering data are then fitted with a fixed radius parameter r_1 for $U_1(r, E)$ and with three other parameters adjustable; the real and the imaginary strengths V_1 and W_1 and the diffuseness parameter a_1. The χ^2 fitting is done for three choices of the radius parameter; r_1=1.3, 1.4, and 1.5 fm. These different choices of the r_1-value are made in order to examine the dependence of the resulting $\sigma_R^{semi-exp}$ on the value of r_1.

As observed in Ref. [1], the values of $\sigma_R^{semi-exp}$ thus extracted for three different r_1-values agree with the average within 1%, implying that $\sigma_R^{semi-exp}$ is determined without much ambiguity. We then identified the average as the final value of $\sigma_R^{semi-exp}$. Using thus determined $\sigma_R^{semi-exp}$, we generated $\sigma_D^{semi-exp}$ by employing Eq. (1). The resultant values of $\sigma_R^{semi-exp}$ and $\sigma_D^{semi-exp}$ are presented in Table I, together with σ_F^{exp} [22], σ_D^{exp} [23], and σ_R^{exp}. As seen from Table I, the values of $\sigma_D^{semi-exp}$ and $\sigma_R^{semi-exp}$ are systematically larger than the corresponding experimental values, except for the lowest energy

Table I: Measured and extracted fusion, DR, and total reaction cross sections for the ^{9}Be+^{208}Pb system. σ_F^{exp} and σ_D^{exp} are from Refs. [22] and [23], respectively. σ_R^{exp} is the sum of σ_F^{exp} and σ_D^{exp}. $\sigma_R^{semi-exp}$ is extracted from the elastic scattering data [21] as explained in the text. $\sigma_D^{semi-exp}$ is then obtained by using Eq. (1).

E_{lab} (MeV)	$E_{c.m.}$ (MeV)	σ_F^{exp} (mb)	σ_D^{exp} (mb)	$\sigma_D^{semi-exp}$ (mb)	σ_R^{exp} (mb)	$\sigma_R^{semi-exp}$ (mb)
38	36.4	10	109	71	119	81
40	38.3	58	180	198	238	256
42	40.3	145	267	320	412	465
44	42.2	248	300	368	548	616
46	44.1	355	300	423	655	778
48	46.0	458	360	541	818	999
50	47.9	580	410	597	990	1177

of E_{cm}=36.4 MeV. The reason why $\sigma_D^{semi-exp}$ is larger than σ_D^{exp} except for the lowest energy may be ascribed to the fact that σ_D^{exp} includes contributions from only breakup, transfer, and incomplete-fusion events [23], but not from inelastic scattering and other simple quasi-elastic processes such as pickups. The difference between σ_R^{exp} and $\sigma_R^{semi-exp}$ becomes larger with energy. It implies that there are more open, but not identified, DR channels as the incident energy increases.

It is worth remarking at this point that there is a reason to question the accuracy of the extracted value of $\sigma_D^{semi-exp}$ at E_{cm}=36.4 MeV. The experimental value of the ratio P_E of the elastic scattering to the Rutherford cross section at the forward angles are systematically larger than unity [21] at this energy. The average value of P_E at small angles is about 1.033. This suggests that there may be a problem in the overall

normalization constant in the measured data. In fact, it is indicated [21] that there are experimental uncertainties of a few percents in the absolute normalization. Even just a few percent uncertainty in the normalization is critical, particularly at low energies in extracting $\sigma_D^{semi-exp}$. In order to confirm this, we have reanalyzed the elastic scattering data by reducing the cross section by a factor of 1.033 so that the values of P_E at forward angles become around unity. A new value of $\sigma_R^{semi-exp}$ thus extracted turns out to be 122 mb, which in turn gives us $\sigma_D^{semi-exp}$=112 mb. This value is significantly greater than 71 mb given in Table I and is also larger than the experimental value of $\sigma_D^{semi-exp}$ = 109 mb. It is thus very plausible that the true values of $\sigma_D^{semi-exp}$ and $\sigma_R^{semi-exp}$ at this energy could be larger than σ_D^{exp} and σ_R^{exp}, respectively. However, in the present χ^2 analyses, use is made of the $\sigma_D^{semi-exp}$ values as listed in Table I.

III. SIMULTANEOUS χ^2 ANALYSES

Simultaneous χ^2-analyses are then performed for two cases of data sets; ($d\sigma_E^{exp}/d\Omega$, σ_D^{exp}, σ_F^{exp}) and ($d\sigma_E^{exp}/d\Omega$, $\sigma_D^{semi-exp}$, σ_F^{exp}) where $d\sigma_E^{exp}/d\Omega$, σ_D^{exp}, and σ_F^{exp} are from the literatures [21, 22, 23]. As mentioned in the Introduction, the former (latter) case with σ_D^{exp} ($\sigma_D^{semi-exp}$) is called the EDF (EF) analysis. In calculating the χ^2 value, we simply assume 1% errors for all the experimental data. The 1% error is roughly the average of errors in the measured elastic scattering cross sections, but it is much smaller than the errors in the DR ($\sim$5%) and fusion ($\sim$10%) cross sections. The choice of the 1% error for DR and fusion cross sections is thus equivalent to increasing the weight for the DR and fusion cross sections in evaluating the χ^2-values by factors of 25 and 100, respectively. Such a choice of errors may be reasonable, since we have only one datum point for each of these cross sections, while there are more than 50 data points for the elastic scattering

cross sections.

A. Necessary Formulae

The optical potential $U(r, E)$ we use in the present work has the following form;

$$U(r; E) = V_C(r) - [V_0(r) + U_F(r; E) + U_D(r; E)], \tag{2}$$

where $V_C(r)$ is the usual Coulomb potential with r_C=1.25 fm and $V_0(r)$ is the bare (Hartree-Fock) nuclear potential. $U_F(r; E)$ and $U_D(r; E)$ are, respectively, fusion and DR parts of the polarization potential [25] originating from couplings to the respective reaction channels. Both $U_F(r; E)$ and $U_D(r; E)$ are complex and their forms are assumed to be of volume-type and surface-derivative-type [8, 26], respectively. $V_0(r)$, $U_F(r; E)$, and $U_D(r; E)$ are explicitly given by

$$V_0(r) = V_0 f(X_0), \tag{3}$$

$$U_F(r; E) = (V_F(E) + iW_F(E)) f(X_F), \tag{4}$$

and

$$U_D(r; E) = (V_D(E) + iW_D(E)) 4a_D \frac{df(X_D)}{dR_D}, \tag{5}$$

where $f(X_i) = [1+\exp(X_i)]^{-1}$ with $X_i = (r-R_i)/a_i$ ($i = 0,\ D$ and F) is the usual Woods-Saxon function, while $V_F(E)$, $V_D(E)$, $W_F(E)$, and $W_D(E)$ are the energy-dependent strength parameters. We assume the geometrical parameters of the real and imaginary potentials are the same, and thus the strength parameters $V_i(E)$ and $W_i(E)$ ($i = F$ or D) are related through a dispersion relation [15],

$$V_i(E) = V_i(E_s) + \frac{E - E_s}{\pi} \mathrm{P} \int_0^\infty dE' \frac{W_i(E')}{(E' - E_s)(E' - E)}, \tag{6}$$

where P stands for the principal value and $V_i(E_s)$ is the value of $V_i(E)$ at a reference energy $E = E_s$. Later, we will use Eq. (6) to generate the final real strength parameters $V_F(E)$ and $V_D(E)$, after $W_F(E)$ and $W_D(E)$ are fixed from χ^2 analyses. Note that the breakup cross section may include contributions from both Coulomb and nuclear interactions, which implies that the direct reaction potential includes effects coming from not only the nuclear interaction, but also the Coulomb interaction.

$V_0(r)$ in Eq. (3) may also have an energy-dependence coming from the nonlocality due to the knockon-exchange contribution. We ignore such effects as they are expected to be small for heavy-ion scattering [27], and employ the real potential parameters used in Ref. [28] assuming that all the unusual features of the potential may be put into the polarization parts, particularly in the DR part. The parameters used for $V_0(r)$ are V_0=18.36 MeV, r_0=1.22 fm, and a_0=0.57 fm [28]. Note that this potential is shallow, which is often required in fitting elastic scattering data of such projectiles as ^{6}Li and ^{9}Be [29].

In performing the optical model calculation, one can evaluate σ_F and σ_D by using the following expression [7, 8, 9, 30]

$$\sigma_i = \frac{2}{\hbar v} < \chi^{(+)} | W_i(r) | \chi^{(+)} > \qquad (i = F \text{ or } D), \tag{7}$$

where $\chi^{(+)}$ is the usual distorted wave function that satisfies the Schrödinger equation with the full optical model potential $U(r, E)$ in Eq. (2). σ_F and σ_D are thus calculated within the same framework as $d\sigma_E/d\Omega$ is calculated. Such a unified description enables us to treat different types of reactions on the same footing.

B. Threshold Energies of Subbarrier Fusion and DR

As in Ref. [1], we also utilize as an important ingredient the so-called threshold energies $E_{0,F}$ and $E_{0,D}$ of subbarrier fusion and DR, respectively, which are defined as zero intercepts of the linear representation of the quantities $S_i(E)$, defined by

$$S_i \equiv \sqrt{E\sigma_i} \approx \alpha_i(E - E_{0,i}) \quad (i = D \text{ or } F), \tag{8}$$

where α_i is a constant. S_i with $i = F$, i.e., S_F is the quantity introduced originally by Stelson *et al.* [20], who showed that in the subbarrier region S_F from the measured σ_F can be represented very well by a linear function of E (linear systematics) as in Eq. (8). In Ref. [26], we extended the linear systematics to DR cross sections. In fact the DR data are also well represented by a linear function.

In Fig. 1(a), we present the experimental $S_F(E)$ and $S_D(E)$. From the zeros of $S_i(E)$, one can deduce $E_{0,D}^{exp}$=30.0 MeV and $E_{0,F}^{exp}$ =35.0 MeV. For both $i = F$ and D, the observed S_i are very well approximated by straight lines in the subbarrier region and thus $E_{0,i}$ can be extracted without much ambiguity. Another determination of $E_{0,D}^{exp}$ can be made by using the semi-experimental DR cross section instead of the experimental DR cross section, as shown in Fig. 1(b). The resultant value, which we shall denote by $E_{0,D}^{semi-exp}$ is found to be $E_{0,D}^{semi-exp} = 32.5$ MeV, close to $E_{0,D}^{exp}$.

$E_{0,i}$ may then be used as the energy where the imaginary potential $W_i(E)$ becomes zero, i.e., $W_i(E_{0,i}) = 0$ [26, 31]. This procedure will be used later in obtaining a mathematical expression for $W_i(E)$.

C. χ^2 Analyses

All the χ^2 analyses performed in the present work are carried out by using $V_0(r)$ as given in Subsec. III A and by using the fixed geometrical parameters for the polarization potentials, r_F=1.40 fm, a_F=0.30 fm, r_D=1.50 fm, and a_D=0.70 fm, which are close to the values used in our previous study [1]. Small changes of these values from the ones used in Ref. [1] are made in order to improve the χ^2-fitting.

As in Ref. [1], the χ^2 analyses are done in two steps; in the first step, all 4 strength parameters, $V_D(E)$, $W_D(E)$, $V_F(E)$ and $W_F(E)$ are varied. In this step, we have been able to fix the strength parameters of the DR potential, $V_D(E)$ and $W_D(E)$, fairly well in the sense that the extracted $V_D(E)$ and $W_D(E)$ turn out to be smooth as functions of E. This is particularly the case for the imaginary strength $W_D(E)$. The values of $V_D(E)$ and $W_D(E)$ are presented in Figs. 2 and 3 by open circles for the EDF and EF cases, respectively. It is remarkable that the resultant $W_D(E)$ can be fairly well represented by the following function of $E(= E_{c.m.})$ (in units of MeV)

$$W_D(E) = \begin{cases} 0 & \text{for } E \leq E_{0,D}^{exp} = 30.0 \\ 0.037(E - 30.0) & \text{for } 30.0 < E \leq 39.0 \\ 0.33 & \text{for } 39.0 < E \end{cases} \tag{9}$$

in the EDF case and

$$W_D(E) = \begin{cases} 0 & \text{for } E \leq E_{0,D}^{semi-exp} = 32.5 \\ 0.052(E - 32.5) & \text{for } 32.5 < E \leq 40.0 \\ 0.39 & \text{for } 40.0 < E \end{cases} \tag{10}$$

in the EF case. Note that the threshold energies where $W_D(E)$ becomes zero are set equal to $E_{0,D}^{exp}$ and $E_{0,D}^{semi-exp}$ as determined in the previous subsection and are indicated by the

open half circles sitting on the axis of $E_{c.m.}$ in Figs. 2 and 3. The dotted lines in the lower panels of Figs. 2 and 3 represent Eqs. (9) and (10), respectively. The dotted curves in the upper panels of Figs. 2 and 3 denote V_D as predicted by the dispersion relation Eq. (6), with $W_D(E)$ given by Eqs. (9) and (10), respectively. As seen, the dotted curves reproduce the open circles fairly well, indicating that $V_D(E)$ and $W_D(E)$ extracted by the χ^2 analyses satisfy the dispersion relation.

In this first step of χ^2 fitting, however, $V_F(E)$ and $W_F(E)$ are not well fixed in the sense that the extracted values fluctuate considerably as functions of E. This is understandable from the expectation that the elastic scattering data can probe most accurately the optical potential in the peripheral region, which is nothing but the region characterized by the DR potential with $r_D = 1.5$ fm. The part of the nuclear potential responsible for fusion with $r_F = 1.4$ fm is thus difficult to pin down in this first step.

In order to obtain more reliable information on V_F and W_F, we have thus performed the second step of the χ^2 analysis. This time, instead of doing a 4-parameter search we use V_D and W_D determined by the first step of χ^2 fitting. But, rather than using V_D and W_D exactly as determined by the χ^2 fitting, we use $W_D(E)$ given by Eqs. (9) and (10) and $V_D(E)$ given by the dispersion relation. We then have performed 2-parameter χ^2 analyses, treating only $V_F(E)$ and $W_F(E)$ as adjustable parameters. The values thus determined are presented in Figs. 2 and 3 by solid circles. As seen, both $V_F(E)$ and $W_F(E)$ are determined to be fairly smooth functions of E. The extracted $W_F(E)$ may be represented by

$$W_F(E) \;=\; \begin{cases} 0 & \text{for } E \le E_{0,F}^{exp} = 35.0 \\ 0.879(E - 35.0) & \text{for } 35.0 < E \le 38.3 \\ 2.90 & \text{for } 38.3 < E \end{cases} \qquad (11)$$

in the EDF case and

$$W_F(E) = \begin{cases} 0 & \text{for } E \leq E_{0,F}^{exp} = 35.0 \\ 0.771(E - 35.0) & \text{for } 35.0 < E \leq 38.5 \\ 2.70 & \text{for } 38.5 < E \end{cases} \quad (12)$$

in the EF case, respectively. As is done for $W_D(E)$, the threshold energy where $W_F(E)$ becomes zero is set equal to $E_{0,F}^{exp}$ and is indicated in Figs. 2 and 3 by the solid half circle on the axis of $E_{c.m.}$. As seen, the $W_F(E)$ values determined by the second χ^2 analyses are fairly well represented by the functions given by Eqs.(11) and (12). Note that the energy variations of $W_F(E)$ and $V_F(E)$ are quite rapid compared to those of $W_D(E)$ and $V_D(E)$, and are similar to those observed in tightly bound projectiles [17, 18, 19].

Using $W_F(E)$ given by Eqs. (11) and (12), one can generate $V_F(E)$ from the dispersion relation. The results are shown by the solid curves in the upper panels of Figs. 2 and 3, which well reproduce the solid circles extracted from the χ^2-fitting. This means that the fusion potential determined from the present analysis satisfies the dispersion relation.

D. Final Calculated Cross Sections in Comparison with the Data

Using $W_D(E)$ given by Eqs. (9) and (10) and $W_F(E)$ given by Eqs. (11) and (12) together with $V_D(E)$ and $V_F(E)$ generated by the dispersion relation Eq. (6), we have performed the final calculations of the elastic, DR and fusion cross sections. Thus, instead of using the potential parameters just as extracted by the χ^2-analyses we have used these dispersive potentials for the final calculations. The results are presented in Figs. 4 and 5 in comparison with the experimental data. All the data are well reproduced by the calculations, though there are subtle differences between the fits obtained by two types of the analyses as will be discussed in detail in Subsec. IV B.

IV. DISCUSSIONS

A. Fusion and DR Potentials

The characteristic features of the polarization potentials determined in the present χ^2 analyses are very much similar to those obtained in our previous analyses [1]. The real and imaginary parts of both fusion and DR potentials satisfy well the dispersion relation, and the fusion potential displays the threshold anomaly. As already presented in Figs. 2 and 3, these features are seen in the strength parameters, $V_F(E)$, $W_F(E)$, $V_D(E)$ and $W_D(E)$.

Another important feature of the extracted potentials is that at the strong absorption radius of R_{sa}=12.3 fm both the real and imaginary parts of the DR potential are considerably greater than those of the fusion potential, although the strength parameters $V_D(E)$ and $W_D(E)$ are smaller than $V_F(E)$ and $W_F(E)$. Thus, the energy dependence of the net polarization potential (sum of the fusion and DR potentials) at R_{sa} becomes dominated by the DR potential which has a relatively smooth energy dependency. Consequently, the net potential does not show such a threshold anomaly as seen in the net potential for systems with tightly bound projectiles [17, 18, 19]. However, after separating the polarization potential into DR and fusion parts, we clearly observe the characteristic threshold anomaly in the fusion potential.

B. Comparison of EDF and EF Cross Sections

Both EDF and EF approaches reproduce the experimental elastic scattering cross sections very well as shown in Fig. 4. The calculated cross sections shown in the left and right panels of Fig. 4 agree well with each other. It may then be naturally expected that

the resultant total reaction cross sections also agree with each other. This is indeed the case; the values of the calculated total reaction cross sections from the EDF approach are approximately equal to those from the EF approach, as shown by the dashed curves in Figs. 5(a) and (b).

Since $\sigma_R^{semi-exp}$ is extracted from the fit to the elastic scattering data, our final calculation results using the dispersive potential naturally reproduce $\sigma_R^{semi-exp}$ as shown by the dotted curves in Fig. 5(b). In the EF case, the calculations also reproduce both DR and fusion cross sections as well. This is, however, not the case for the EDF approach; calculations using the dispersive potential somewhat overestimates the experimental data of all three cross sections as Fig. 5(a) shows.

It may thus be concluded that the overall fit to the data obtained in the EF case is better than the EDF case and that the main source of problems in getting a good overall fit in the EDF case comes from inconsistency between the elastic scattering [21] and the DR reaction [23] data; the elastic scattering data require more absorption (larger total reaction cross section) than what the measured total absorption (reaction) cross sections tell us. In view of this, it is important that measurements be made of inelastic scattering and some other quasi-elastic reactions which are not taken into account in the total DR cross section used in the present analyses.

C. Effects of Breakup on Fusion

We now turn to the effect of breakup on the fusion cross section. As has been argued, there are two competing physical effects of breakup on the fusion cross section, σ_F. The first is the lowering of the fusion barrier, which tends to enhance σ_F. The other is the removal of flux from the elastic into the breakup channel, which suppresses σ_F. Since the

breakup channel dominates DR, these two competing breakup effects may be represented by the real ($V_D(r;E)$) and the imaginary ($W_D(r;E)$) parts of the DR potential; $V_D(r,E)$ can describe precisely the effect of lowering the barrier, while $W_D(r,E)$ the removal of the flux from the elastic channel.

To see the effects quantitatively, we have introduced in Ref. [1] the following suppression factor R^{th},

$$R^{th} = \sigma_F/\sigma_F(V_D = W_D = 0), \tag{13}$$

where $\sigma_F(V_D = W_D = 0)$ is σ_F obtained by setting $V_D = W_D = 0$, i.e., neglecting both barrier-lowering and flux loss effects, while σ_F is our final calculated cross section that includes both V_D and W_D. In the above-barrier region, R^{th} becomes almost constant and here we present just the average of the R^{th}-values at three highest energies considered in the present study. The values are 0.87 and 0.82 for the EDF and EF cases, respectively. Setting $V_D = 0$ reduces σ_F, while setting $W_D = 0$ increases σ_F. Thus, the fact that the R^{th}-values are smaller than unity indicates that the flux loss effect surpasses the barrier-lowering effect in the above barrier region. The theoretical values may be compared with the experimental values of R^{exp}=0.79, where R^{exp} is defined as

$$R^{exp} = \sigma_F^{exp}/\sigma_F(V_D = W_D = 0). \tag{14}$$

by using $\sigma_F(V_D = W_D = 0)$ fixed from the EF case. R^{exp} in the EDF case is 0.77, quite close to R^{exp} in the EF case.

Note that the theoretical suppression factor R^{th}=0.82 in the case of EF agrees very well with the experimental value of R^{exp}=0.79. It is natural because the calculated σ_F agrees with σ_F^{exp} in the EF case as shown in Fig. 5(b). Similarly, the difference between R^{th}=0.87 and R^{exp}=0.77 in the EDF case originates from the discrepancy between σ_F^{exp}

and the calculated σ_F, seen in Fig. 5(a). In either case, both R^{th} and R^{exp} are consistently and considerably smaller than unity, implying that the observed suppression of σ_F can be ascribed to the flux loss in the elastic channel to breakup. A similar result was also obtained in Ref. [1].

Although breakup (or DR) is the dominant factor in the suppression of σ_F in the above barrier region, this is not the case in the sub-barrier region, where the neutron flow affects fusion dominantly [20], generally enhancing the sub-barrier fusion. In Ref. [1], it was proposed that a good measure for the sub-barrier fusion enhancement is the quantity Δ defined as

$$\Delta = V_B - E_{0,F}, \tag{15}$$

where V_B is the Coulomb-barrier height and $E_{0,F}$ is the sub-barrier threshold energy discussed in Subsec. II B. In Ref. [1], it is demonstrated that Δ is very well proportional to the neutron transfer Q-value.

D. Comments on the Analyses of the ^{9}Be+^{209}Bi System Reported in Ref. [1]

In Ref. [1], we presented our analyses on the ^{9}Be+^{209}Bi system using only the elastic scattering [5] and fusion cross section data [6] (the EF type analysis). Since the target nucleus ^{209}Bi differ from ^{208}Pb only by one proton, it is naturally expected that the experimental cross sections for the two systems should be very similar. This is indeed the case for the elastic scattering cross sections; no noticeable difference can be found in the data measured for the Pb target [21] and Bi target [5]. In contrast to this, the values of the fusion cross section for the Bi target we used from Ref. [6] at the time of our analyses [1] are significantly larger than those for the Pb target reported in Ref. [4].

Recently, however, the fusion cross sections for the Bi target are revised [32], and the revised values are now very much the same as those of the Pb target.

Due to this change in the experimental values of σ_F^{exp} for ^{209}Bi, we have repeated our previous analyses for ^{9}Be + ^{209}Bi system, obtaining now essentially the same results as in the present work for ^{9}Be + ^{208}Pb. Therefore, we take this opportunity to revise our previous values of the suppression factor R; the new theoretical value obtained with the revised data is R^{th}=0.81, which can be compared with the new experimental value of R^{exp}=0.79. The corresponding values reported previously in Ref. [1] were R^{th}=0.89 and R^{exp}=0.92.

V. CONCLUSIONS

In summary, we have carried out simultaneous χ^2 analyses of elastic scattering, DR (breakup plus incomplete fusion), and fusion cross sections for the ^{9}Be+^{208}Pb system at near-Coulomb-barrier energies within the framework of an extended optical model that introduces the DR and fusion potentials. Two types of analyses are made; one using the experimental DR cross section σ_D^{exp} (EDF case), and the other using the semi-experimental DR cross section $\sigma_D^{semi-exp}$ (EF case), together with the measured elastic scattering and fusion cross sections for both cases. In the second type of the analyses, $\sigma_D^{semi-exp}$ is first extracted from simple optical model fits to the elastic scattering data only. The extracted $\sigma_D^{semi-exp}$ are found to be significantly larger than σ_D^{exp}. In spite of this difference between σ_D^{exp} and $\sigma_D^{semi-exp}$, the resultant DR and fusion potentials show common features that they satisfy fairly well the dispersion relation [15] and the fusion potentials show the threshold anomaly as seen in the potentials for systems with tightly bound projectiles [16, 17, 18, 19].

For both EDF and EF cases the elastic scattering cross sections are equally well reproduced. However, the calculated DR, fusion, and total reaction cross sections fit the corresponding experimental data well in the EF case, but not in the EDF case. In the latter case, the calculations overestimate significantly the experimental DR, fusion, and total reaction cross sections. This is because there are some reaction channels that are not taken into consideration in the present experimental DR data.

Thus as far as we don't have comprehensive σ_D^{exp} available, the EF analysis gives us better overall results than the EDF analysis. We believe that if the cross section of inelastic scattering and some other missing reactions that are not taken into account in the present data of σ_D^{exp} [23] are measured and used in the analyses, both types of analyses will lead to equally good fit to the data. It is thus highly desirable that such DR data will be measured in near future in order to test our expectation and thus to justify the validity of the EF method proposed in Ref. [1].

The authors sincerely thank Drs. Woolliscroft and Dasgupta for their kindly sending the numerical values of the data they took. SWH thank TRIUMF for the hospitality where part of the work is done. The work is supported by the Basic Research Program of the KOSEF, Korea (Grant No. R05-2003-000-12088-0).

[1] W. Y. So, S. W. Hong, B. T. Kim, and T. Udagawa, Phys. Rev. C **69**, 064606 (2004).

[2] N. Keeley, S. J. Bennett, N. M. Clarke, B. R. Fulton, G. Tungate, P. V. Drumm, M. A. Nagarajan, and J. S. Lilly, Nucl. Phys. **A571**, 326 (1994).

[3] Y. W. Wu, Z. H. Liu, C. J. Lin, H. Q. Zhang, M. Ruan, F. Yang, Z. C. Li, M. Trotta, and K. Hagino, Phys. Rev. C. **68**, 044605 (2003).

[4] M. Dasgupta *et al.*, Phys. Rev. C **66**, 041602(R) (2002).

[5] C. Signorini *et al.*, Phys. Rev. C **61**, 061603(R) (2000).

[6] C. Signorini *et al.*, Eur. Phys. J. A **5**, 7 (1999) and private communications.

[7] T. Udagawa, B. T. Kim, and T. Tamura, Phys. Rev. C **32**, 124 (1985); T. Udagawa and T. Tamura, Phys. Rev. C **29**, 1922 (1984).

[8] S.-W. Hong, T. Udagawa, and T. Tamura, Nucl. Phys. **A491**, 492 (1989).

[9] T. Udagawa, T. Tamura, and B. T. Kim, Phys. Rev. C **39**, 1840 (1989); B. T. Kim, M. Naito, and T. Udagawa, Phys. Lett. B **237**, 19 (1990).

[10] R. H. McCamis *et al.*, Can. J. Phys. **64**, 685 (1986).

[11] T. Eliyakut-Roshko, R. H. McCamis, W. T. H. van Oers, R. F. Carlson, and A. J. Cox, Phys. Rev. C **51**, 1295 (1995).

[12] A. Auce *et al.*, Phys. Rev. C **53**, 2919 (1996).

[13] P. Singh, A. Chatterjee, S. K. Gupta, and S. S. Kerekatte, Phys. Rev. C. **43**, 1867 (1991).

[14] J. J. Kolata *et al.*, Phys. Rev. Lett. **81**, 4580 (1998).

[15] C. C. Mahaux, H. Ngo, and G. R. Satchler, Nucl. Phys. **A449**, 354 (1986); Nucl. Phys. **A456**, 134 (1986).

[16] M. A. Nagarajan, C. C. Mahaux, and G. R. Satchler, Phys. Rev. Lett. **54**, 1136 (1985).

[17] A. Baeza, B. Bilwes, J. Diaz, and J. L. Ferrero, Nucl. Phys. **A419**, 412 (1984).

[18] J. S. Lilley, B. R. Fulton, M. A. Nagarajan, I. J. Thompson, and D. W. Banes, Phys. Lett.

151B, 181 (1985).

[19] B. R. Fulton, D. W. Banes, J. S. Lilley, M. A. Nagarajan, and I. J. Thompson, Phys. Lett. **162B**, 55 (1985).

[20] P. H. Stelson, Phys. Lett. B **205**, 190 (1988); P. H. Stelson, H. J. Kim, M. Beckerman, D. Shapira, and R. L. Robinson, Phys. Rev. C **41**, 1584 (1990).

[21] R. J. Woolliscroft *et al.*, Phys. Rev. C **69**, 044612 (2004).

[22] M. Dasgupta *et al.*, Phys. Rev. Lett **82**, 1395 (1999).

[23] R. J. Woolliscroft *et al.*, Phys. Rev. C **68**, 014611 (2003).

[24] R. A. Broglia and A. Winther, *Heavy Ion Reactions Lecture Note Volume I: Elastic and Inelastic Reactions*, p165, (Benjamins, London, 1981).

[25] W. G. Love, T. Terasawa, and G. R. Satchler, Nucl. Phys. A **291**, 183 (1977).

[26] B. T. Kim, W. Y. So, S. W. Hong, and T. Udagawa, Phys. Rev. C. **65**, 044607 (2002).

[27] G. R. Satchler, *Introduction to Nuclear Reactions*, (Wiley, New York, 1980).

[28] H. Wojciechowski, L. R. Medsker, and R. H. Davis, Phys. Rev. C **16**, 1767 (1977).

[29] G. R. Satchler and W. G. Love, Phys. Rep. **55**, 183 (1979).

[30] M. S. Hussein, Phys. Rev. C **30**, 1962 (1984).

[31] B. T. Kim, W. Y. So, S. W. Hong, and T. Udagawa, Phys. Rev. C. **65**, 044616 (2002).

[32] C. Signorini *et al.*, Prog. Theor. Phys. **107**, 1 (2002).

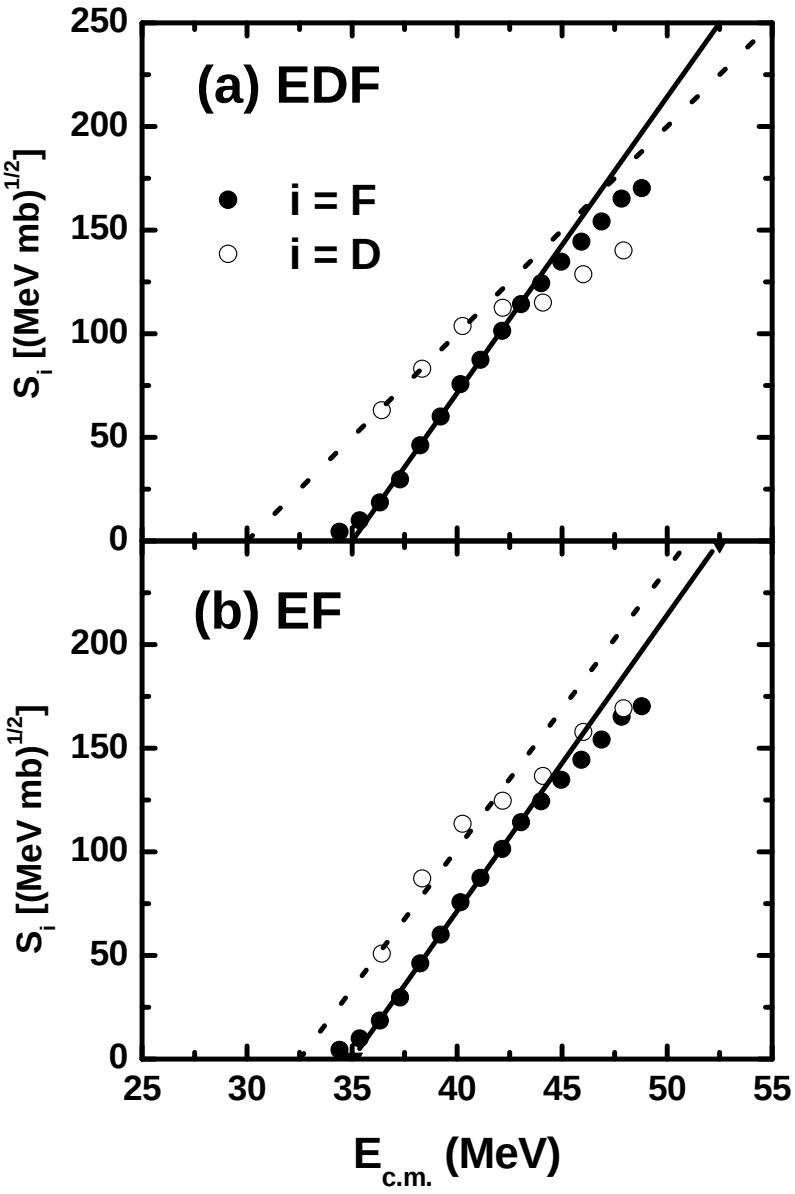

Fig. 1: The Stelson plot of $S_i = \sqrt{E_{c.m.}\sigma_i}$ for DR ($i = D$, open circles) and fusion ($i = F$, solid circles) cross sections with (a) the experimental and (b) the semi-experimental DR cross sections. The straight lines are drawn to show the extraction of the threshold energies $E_{0,i}$.

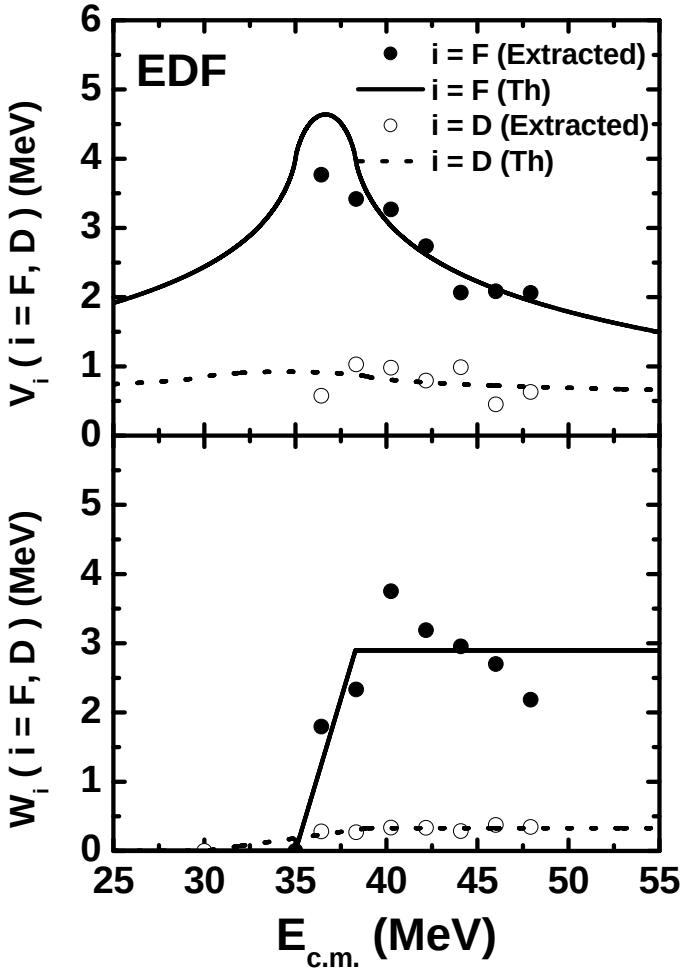

Fig. 2: The strength parameters V_i (upper panel) and W_i (lower panel) for $i = D$ and F as functions of $E_{c.m.}$ in the EDF case. The open and solid circles are the strength parameters for $i = D$ and F, respectively. The dotted and solid lines in the lower panel denote W_D and W_F from Eqs. (9) and (11), respectively, while the dotted and solid curves in the upper panel represent V_D and V_F calculated by using the dispersion relation of Eq. (6) with W_i given by Eqs. (9) and (11). The reference energies, $V_F(E_s)$ and $V_D(E_s)$, are chosen as 4.0 MeV and 0.85 MeV, respectively.

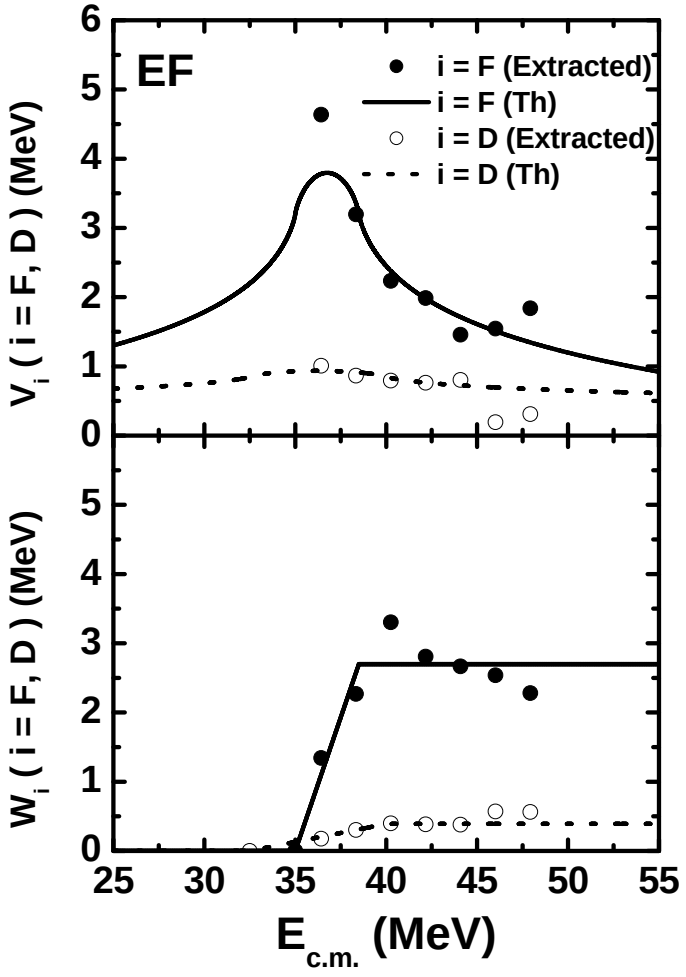

Fig. 3: The same as in Fig. 2, but for the EF case. The dotted (solid) line in the lower panel denotes W_D (W_F) from Eq. (10) (Eq. (12)). The dotted (solid) curve in the upper panel represents V_D (V_F) obtained by the dispersion relation. The reference energy E_s for $V_F(E_s)$ and $V_D(E_s)$, are taken as 3.2 MeV and 0.85 MeV, respectively.

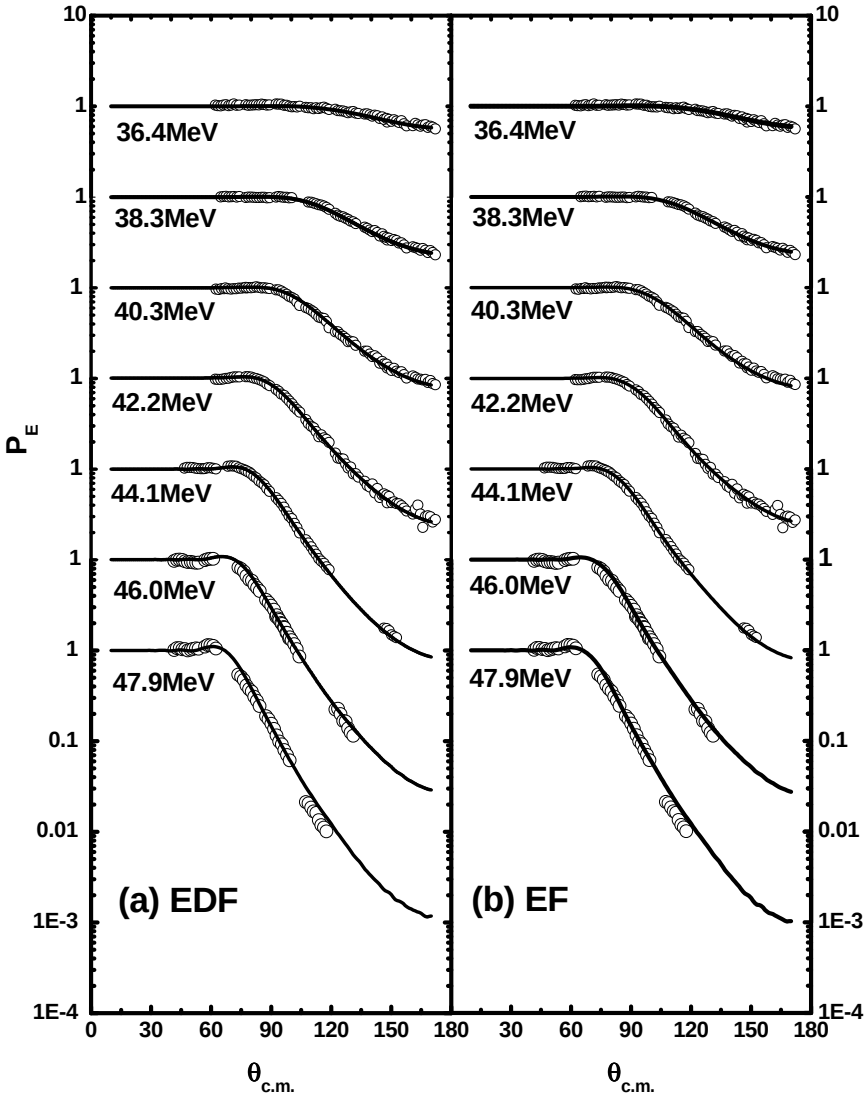

Fig. 4: Ratios of the elastic scattering cross sections to the Rutherford cross section calculated with our final dispersive optical potential for (a) the EDF and (b) the EF cases are shown in comparison with the experimental data. The data are taken from Ref. [21].

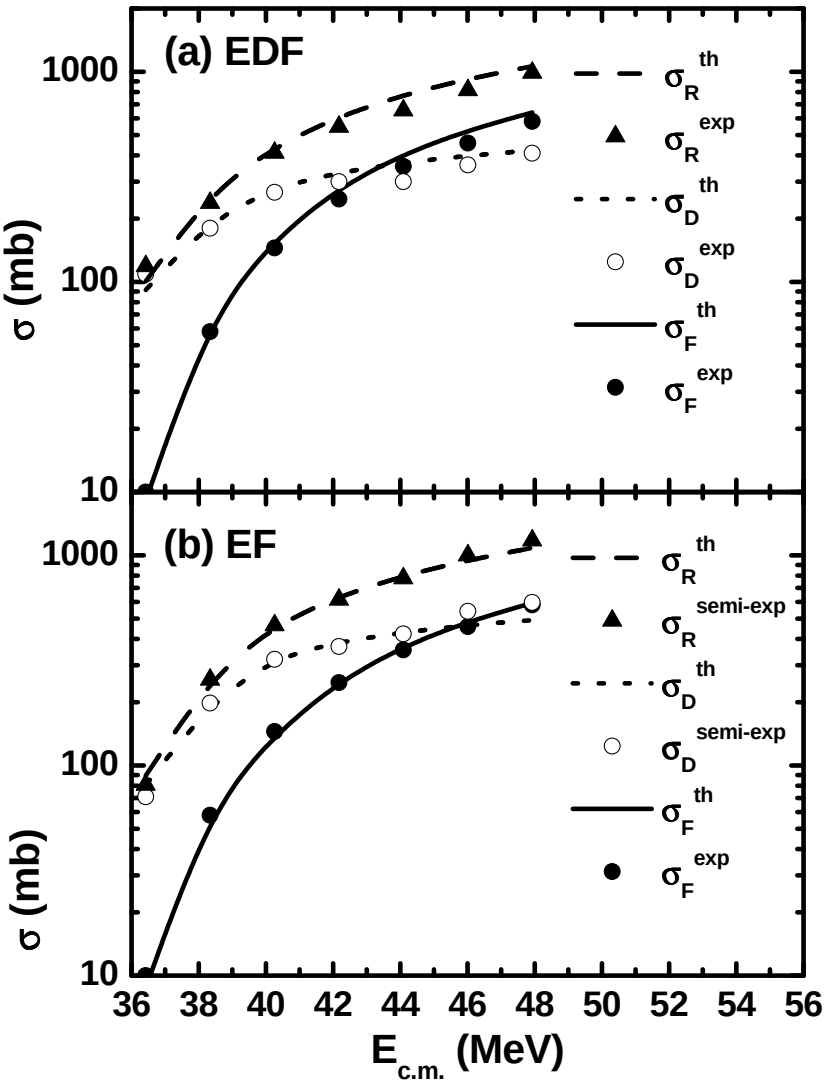

Fig. 5: DR and fusion cross sections calculated with our final dispersive optical potential for the (a) EDF and (b) EF cases are shown in comparison with the experimental data. $\sigma_D^{semi-exp}$ denoted by the open circles in EF case are obtained as described in Sec.II. σ_D^{exp} denoted by the open circles in EDF case are the experimental DR cross sections [23]. The fusion data are from Ref. [22].

FIGURE CAPTIONS

Fig. 1. The Stelson plot of $S_i = \sqrt{E_{c.m.}\sigma_i}$ for DR ($i = D$, open circles) and fusion ($i = F$, solid circles) cross sections with (a) the experimental and (b) the semi-experimental DR cross sections. The straight lines are drawn to show the extraction of the threshold energies $E_{0,i}$.

Fig. 2. The strength parameters V_i (upper panel) and W_i (lower panel) for $i = D$ and F as functions of $E_{c.m.}$ in the EDF case. The open and solid circles are the strength parameters extracted by χ^2-fitting for $i = D$ and F, respectively. The dotted and solid lines in the lower panel denote W_D and W_F from Eqs. (9) and (11), respectively, while the dotted and solid curves in the upper panel represent V_D and V_F calculated by using the dispersion relation of Eq. (6) with W_i given by Eqs. (9) and (11). The reference energy E_s for $V_F(E_s)$ and $V_D(E_s)$, are chosen as 4.0 MeV and 0.85 MeV, respectively.

Fig. 3. The same as in Fig. 2, but for the EF case. The dotted (solid) line in the lower panel denotes W_D (W_F) from Eq. (10) (Eq. (12)). The dotted (solid) curve in the upper panel represents V_D (V_F) obtained by the dispersion relation. The reference energy E_s for $V_F(E_s)$ and $V_D(E_s)$, are taken as 3.2 MeV and 0.85 MeV, respectively.

Fig. 4. Ratios of the elastic scattering cross sections to the Rutherford cross section calculated with our final dispersive optical potential for (a) the EDF and (b) the EF cases are shown in comparison with the experimental data. The data are taken from Ref. [21].

Fig. 5. DR and fusion cross sections calculated with our final dispersive optical potential for the (a) EDF and (b) EF cases are shown in comparison with the experimental data. $\sigma_D^{semi-exp}$ denoted by the open circles in EF case are obtained as described in Sec.II. σ_D^{exp} denoted by the open circles in EDF case are the experimental DR cross sections [23]. The fusion data are from Ref. [22].